frontiers | Frontiers in Earth Science

TYPE Original Research
PUBLISHED 06 February 2025
DOI 10.3389/feart.2025.1505090

OPEN ACCESS

EDITED BY
Xin Sun,
Sinopec Matrix Co., Ltd., China

REVIEWED BY
Yumao Pang,
Shandong University of Science and Technology, China
Shib Sankar Ganguli,
National Geophysical Research Institute (CSIR), India

*CORRESPONDENCE
Yuanhao Zhang,
13352592272@163.com
Zhenxue Jiang,
jiangzx@cup.edu.cn

RECEIVED 02 October 2024
ACCEPTED 17 January 2025
PUBLISHED 06 February 2025

CITATION
Wang J, Shao H, Zhang Y, Jiang Z, Gao B, Li L, Pan H, Wang H, Lu X, Qiu H, He X and Zhang C (2025) Multifractal characteristics of pore structure in the terrestrial shale reservoirs of the Lianggaoshan formation in northeast sichuan basin and its geological significance. *Front. Earth Sci.* 13:1505090. doi: 10.3389/feart.2025.1505090

Multifractal characteristics of pore structure in the terrestrial shale reservoirs of the Lianggaoshan formation in northeast sichuan basin and its geological significance

Jiping Wang[1,2], Hongmei Shao[1,2], Yuanhao Zhang[3,4]*, Zhenxue Jiang[3,4]*, Bo Gao[1,2], Lingling Li[1,2], Huifang Pan[1,2], Haonan Wang[1,2], Xi Lu[1,2], Hengyuan Qiu[1,2], Xiaobiao He[3,4] and Chengju Zhang[3,4]

[1]State Key Laboratory of Continental Shale Oil, Daqing, China, [2]PetroChina Daqing Oilfield Exploration and Development Research Institute, Daqing, China, [3]State Key Laboratory of Petroleum Resources and Engineering, China University of Petroleum (Beijing), Beijing, China, [4]Unconventional Oil and Gas Science and Technology Research Institute, China University of Petroleum, Beijing, China

The exploration of shale oil resources in the Lianggaoshan Formation of the Jurassic System in the Sichuan Basin has made significant progress in recent years, revealing a vast resource potential. This study focuses on the upper Lianggaoshan Formation, employing low-temperature gas adsorption, high-pressure mercury intrusion, and nuclear magnetic resonance techniques to systematically characterize the pore structure of various lithofacies shales. Furthermore, the pore structure heterogeneity and its controlling factors were investigated through the integration of multifractal theory. Result indicate that high-organic laminated felsic shale exhibit well-developed micropores with a simple and uniform pore structure, making them ideal for shale oil accumulation. Medium-organic bedded felsic shale, also exhibiting laminated and feldspathic textures, possess a more complex mesoporous structure that facilitates hydrocarbon enrichment, but their high heterogeneity presents challenges for exploration and development. Low-organic massive argillaceous siltstone with low organic content demonstrates a complex macroporous structure and high heterogeneity, potentially limiting effective hydrocarbon recovery. Lastly, the pore structure of massive fine-silt sandstone exhibits a high degree of complexity and heterogeneity, revealing the significant influence of quartz and clay mineral interactions on pore development. These findings advance the understanding of shale pore structure and its impact on hydrocarbon enrichment and recovery in the Lianggaoshan Formation, and offer valuable guidance for optimizing "sweet spot" selection. Furthermore, the methodologies and insights presented here are broadly applicable to unconventional resource exploration and development in similar geological

settings globally, providing new ideas for researchers studying shale reservoir pore systems.

KEYWORDS

Lianggaoshan formation, shale oil, nuclear magnetic resonance, multifractal characteristics, pore structure

1 Introduction

Shale oil and gas represent a significant unconventional hydrocarbon resource with substantial global development potential (Stevens et al., 2013; Li et al., 2021; Yuan et al., 2024). Recent years have seen significant advances in the exploration of lacustrine shale oil wihin multiple Chinese basins, including the Bohai Bay Basin and the Songliao Basin, underscoring the strategic importance of this resource for enhancing domestic oil and gas reserves and production (Wang et al., 2022a). In the Sichuan Basin, the exploration of Jurassic Lianggaoshan Formation shale oil resources has progressed through three distinct phases: conventional oil and gas, tight oil and gas, and shale oil and gas. This transition from traditional sandstone and carbonate reservoirs to lacustrine shale has resulted in numerous significant discoveries (Chen et al., 2024a).

The Jurassic Lianggaoshan Formation shale oil resources in the Sichuan Basin are now estimated to exceed 200 million tons, with multiple wells, including PA1 Well, demonstrating substantial oil and gas production within the Lianggaoshan Formation shale. This confirms the region's abundance of shale oil resources and promising exploration potential (Chen et al., 2024a). However, the shales of the Liangaoshan Formation are highly inhomogeneous, with a variety of lithological assemblages, including gray-black shale, Shell-type shale, siltstone and fine sandstone (He et al., 2022; Fang et al., 2024). These lithologic assemblages significantly control the development and oil-bearing potential of shale reservoirs. And there are notable differences in shale oil enrichment patterns and main controlling factors under various lithologic combination assemblages (Hu et al., 2022; Yuan et al., 2024). This complexity poses challenges for effective "sweet spot" selection and efficient development.

Pore structure is pivotal to shale oil accumulation and mobility (Wang et al., 2021; Cao et al., 2024; Chang et al., 2024a; Zhang et al., 2024b). The pore-throat structure of shale reservoirs not only influences shale oil accumulation but also directly impacts its productivity. Advances in exploration technologies have led to the widespread application of advanced techniques, including nitrogen and carbon dioxide adsorption, small-angle X-ray scattering (SAXS), field-emission scanning electron microscopy (FE-SEM), focused ion beam scanning electron microscopy (FIB-SEM), low-temperature gas adsorption, high-pressure mercury intrusion porosimetry, and nuclear magnetic resonance (NMR) spectroscopy, for the qualitative and quantitative characterization of complex shale pore structures (Vafaie et al., 2015; Jiang et al., 2022; Zhao et al., 2022; Bal et al., 2023). Among these, NMR spectroscopy has become a crucial method for investigating shale reservoir pore structure due to its ability to rapidly and nondestructively measure porosity and pore size distribution (Fleury et al., 2022; Cai et al., 2023; Zhang et al., 2023b).

Combined with fractal theory, NMR exhibits a significant advantage in studying reservoir heterogeneity (Daigle et al., 2014; Zhou and Kang, 2016; Li et al., 2018). Fractal theory, especially multifractal theory, presents a novel approach to characterizing the heterogeneity of complex pore structures (Rahner et al., 2018; Turlapati et al., 2020; Chang et al., 2022). Unlike the limitations of single-fractal models, multifractal theory partitions complex pore structures into multiple regions with the same singularity strength and generalized fractal dimension. Analysis of these regions provides a comprehensive characterization of pore structure heterogeneity (Han et al., 2024). The application of multifractal theory to the study of rock pore structure has expanded significantly in recent years (Vega and Jouini, 2015; Dimri and Ganguli, 2019; Jouini et al., 2022). For example, Zhao et al. (2017) u employed multifractal analysis to demonstrate a positive correlation between clay mineral content and pore structure heterogeneity. Meanwhile, Zheng et al. (2019) proposed a novel T_2 cutoff value algorithm based on multifractal parameters, enabling more precise delineation of shale fluid occurrence states. Zhang et al. (2023a) used NMR multifractal theory to develop a predictive model for the free-fluid volume index, subsequently quantifying fluid mobility in the studied rocks.

This study focuses on the Jurassic Lianggaoshan Formation shale in the Yilong-Pingchang area of the Sichuan Basin, aiming to systematically characterize the pore structure features of the shale across multiple scales and to reveal its heterogeneity. Experimental methods including low-temperature gas (N_2, CO_2) adsorption, high-pressure mercury intrusion, scanning electron microscopy, and nuclear magnetic resonance were employed to qualitatively and quantitatively analyze the multiscale pore structure of the shale. The box-counting method was applied to quantify the multifractal characteristics of shales from different lithofacies. Finally, the relationships between pore structure parameters, lithological characteristics, and multifractal dimensions in different lithofacies were examined. Through these analyses, this study seeks to provide a new theoretical foundation and data support for shale reservoir evaluation and heterogeneity research in the study area.

2 Geological setting

The Sichuan Basin's complex internal tectonic structure reflects its development through multiple tectonic deformations. Significant uplift during the Yanshanian Movement led to differential basin evolution. Subsequently, the Himalayan folding deformation further shaped the basin into six secondary tectonic units extending east to west: the eastern Sichuan high-angle tectonic belt, the southern Sichuan low-angle tectonic belt, the northern Sichuan gentle tectonic belt, the central Sichuan

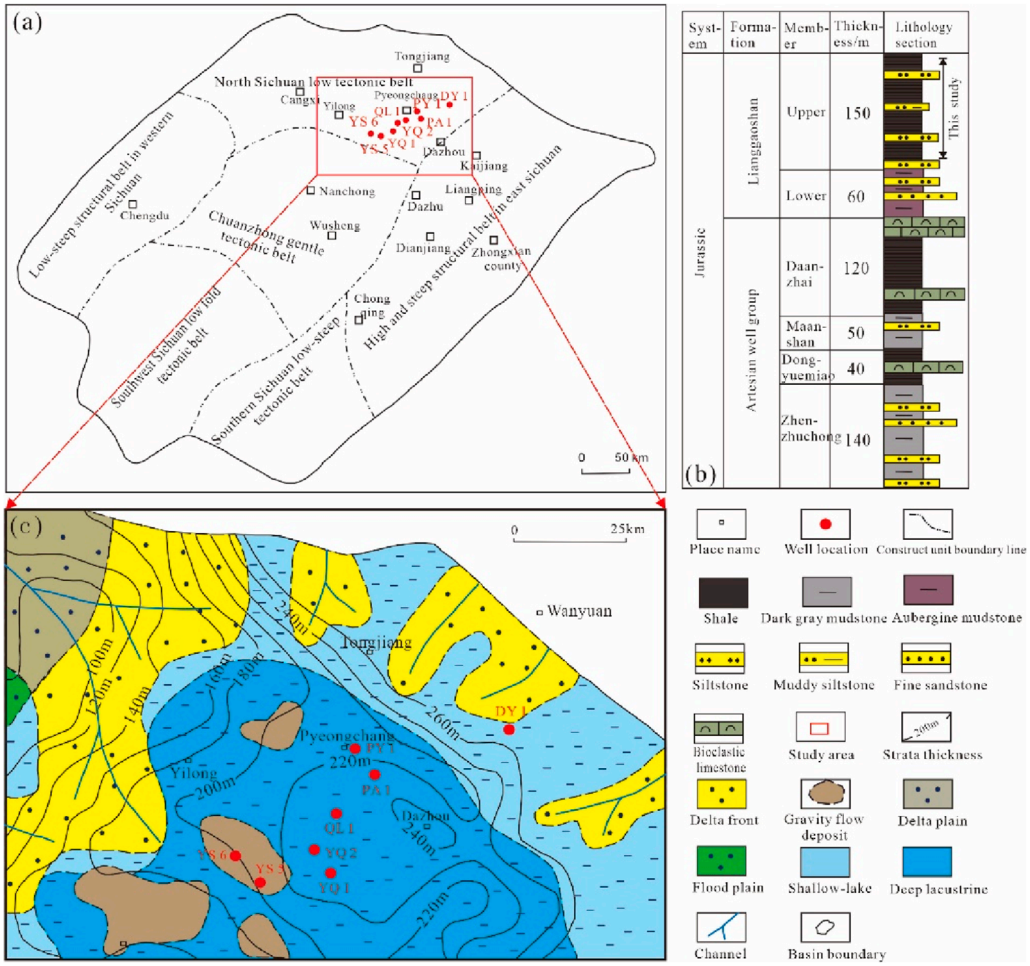

FIGURE 1
Geological map of the research area. **(A)** Geological overview and study area location of sichuan basin; **(B)** Comprehensive column chart of Jurassic strata; **(C)** Sedimentary facies map of Lianggaoshan formation in northeastern Sichuan [modified from Cheng et al. (2023); Wang et al. (2024)].

gentle belt, the southwestern Sichuan gentle folded tectonic belt, and the western Sichuan low-angle tectonic belt (Figure 1A) (Chen et al., 2020). The Yilong-Pingchang area is situated within the transition zone between the northern Sichuan gentle tectonic belt and the central Sichuan gentle tectonic belt (Yu et al., 2022). The basin encompasses over 20 oil-bearing formations, with the Jurassic formations representing the shallowest known oil-bearing stratigraphic unit. The Jurassic is characterized by widespread development of thick terrestrial mudstone-shale sequences, primarily within the Lower Jurassic Lianggaoshan and Ziliujing Formations (Wang et al., 2024). The Lianggaoshan Formation, with a total thickness of 210 m, is further subdivided into an upper (Liangshang) and lower (Liangxia) section based on sedimentary cycles (Cheng et al., 2023). This study focuses on the Liangshang section, which has a thickness of 150 m (Figure 1B).

The study area is dominated by delta-lake deposits and has undergone three periods of lacustrine basin expansion (Cheng et al., 2023). The Liangshang depositional period primarily occurred during the third lake basin expansion, encompassing a complete cycle of lake transgression and regression. This resulted in the formation of coastal and delta-front subfacies, with predominantly dark shale, siltstone, and mudstone-siltstone lithologies (Hu et al., 2021; Wang et al., 2022b).

3 Experimental methods and multifractal theory

3.1 Samples

Shale samples from the upper section of the Lianggaoshan Formation were selected for this study, encompassing a range of lithologies including shell limestone, mudstone-siltstone, siltstone, and fine sandstone, representing the typical lithologies of the Liangshang. Samples were sectioned parallel to bedding planes and prepared according to the specific requirements of each analytical technique. These techniques included total organic carbon (TOC) analysis, Rock-Eval pyrolysis (R_o), X-ray Diffraction (XRD), Field Emission Scanning Electron Microscopy (FE-SEM), CO_2 Gas Adsorption (GO_2GA), Low-Temperature N_2 Adsorption (LTN_2A), Mercury Intrusion Porosimetry (MIP), and NMR.

3.2 Experimental methods

3.2.1 CO_2GA & LTN_2A

Low-temperature nitrogen adsorption and CO_2 adsorption experiments were performed using an ASAP2460 automated surface area and pore size analyzer. The experiments were conducted according to industry standards GB/T 21650.3-2011 and GB/T 19587-2017. Samples with a particle size of 60-80 mesh were dried, degassed, and then analyzed in the instrument. The mesoporous and microporous volumes were determined using the Barrett–Joyner–Halenda (BJH) model and the Density Functional Theory (DFT) model, respectively (Pang et al., 2021).

3.2.2 MIP

MIP experiments were carried out using an Auto Pore IV 9500 automated mercury porosimeter. Cubic samples with a volume of 1 cm^3 were prepared, dried, and then placed in the instrument for testing. The experiments adhered to the GB/T 29171-2012 standard for determining the capillary pressure curves of rocks, resulting in the acquisition of mercury intrusion and extrusion curves for the shale samples. The Washburn equation was then used to calculate the macropore volume.

The Washburn Equation 1 describes the relationship between time and capillary height:

$$t = \frac{2\eta h^2}{cr\sigma \cos\theta} \tag{1}$$

Here, c represents the capillary shape coefficient, r denotes the average capillary radius, σ signifies the surface tension of the liquid, η represents the viscosity of the liquid, and h indicates the capillary height.

3.2.3 NMR

NMR measurements were conducted using a MesoMR23-060H-I NMR core analyzer, employing cylindrical samples with a diameter of 2.5 cm and a length of 5 cm, representing distinct lithologies. T_2 spectra were acquired for each sample, following the guidelines outlined in the 4SY-T6490-2014 standard for laboratory measurements of rock NMR parameters.

The transverse relaxation time (T_2) in NMR is influenced by three key parameters: surface relaxation time (T_{2s}), free relaxation time (T_{2B}), and diffusion relaxation time (T_{2D}), as expressed by:

$$\frac{1}{T_2} = \frac{1}{T_{2s}} + \frac{1}{T_{2B}} + \frac{1}{T_{2D}} \tag{2}$$

Due to the prevalence of nanopores within shale, surface relaxation time plays a dominant role in determining the overall T_2 relaxation behavior. The above Equation 2 can be rewritten as:

$$\frac{1}{T_2} = \frac{1}{T_{2s}} \tag{3}$$

Surface relaxation is directly proportional to the specific surface area of the shale, and based on Equation 3, we can derive:

$$\frac{1}{T_2} = \frac{1}{T_{2s}} = \rho_2 \frac{S}{V} \tag{4}$$

Where S represents the pore surface area (m^2), V denotes the pore volume (m^3), S/V represents the specific surface area of the shale, and ρ_2 represents the surface relaxation rate (μm/ms).

Here, S/V is equivalent to F/r, where r represents the pore radius and F characterizes the pore shape. Consequently, Equation 4 can be rewritten as:

$$r = \rho_2 F T_2 \tag{5}$$

Equation 5 establishes a direct relationship between pore radius and NMR T_2 spectra, enabling quantitative characterization of the pore size distribution within shale samples.

3.2.4 FE-SEM

FE-SEM analysis was performed using a FEI Quanta FEG450 instrument. Shale samples underwent argon ion polishing to prepare 1 cm cubic specimens for examination. Backscatter imaging was conducted to observe pore types and their spatial distribution, adhering to the SY/T 5162-2014 standard for scanning electron microscopy analysis of rock samples.

3.2.5 TOC & Ro

Total organic carbon (TOC) content was determined using a CS-230 carbon-sulfur analyzer. Samples were sieved to a particle size less than 100 mesh before analysis. TOC values were obtained for each shale sample, adhering to the GB/T 19145-2003 standard for the determination of total organic carbon in sedimentary rocks.

Vitrinite reflectance measurements were conducted using a polarizing microscope equipped with a photometer. Samples were crushed and sieved to a size less than 2 mm, followed by polishing and drying for 12 h before analysis. The SY/T 5124-2012 standard was adhered to for these measurements.

3.2.6 XRD

Whole-rock X-ray diffraction (XRD) analysis was conducted using a Shimadzu XRD-6100 instrument to determine the mineral composition of the shale samples. Prior to analysis, the samples were pulverized and ground. The analysis adhered to the SY/T 5163-2018 standard for X-ray diffraction analysis of clay minerals and common non-clay minerals in sedimentary rocks.

3.3 Multifractal theory

Based on the T_2 spectra obtained from one-dimensional NMR experiments, the multifractal dimension of the NMR data under different conditions was calculated using the box-counting method. The core T_2 spectra were normalized and accumulated, then divided into N equal parts (ε). The entire dataset underwent interpolation, and the probability mass function of the ith segment can be expressed in Equation 6 (Zhang et al., 2024a):

$$P_i(\varepsilon) = \frac{N_i(\varepsilon)}{\sum_{i=1}^{N(\varepsilon)} N_i(\varepsilon)} \tag{6}$$

Here, $N_i(\varepsilon)$ represents the cumulative porosity or volume of pores within the ith partition, while $P_i(\varepsilon)$ denotes the probability mass function.

Within the framework of multifractal theory, the probability mass function $P_i(\varepsilon)$ exhibits a power-law relationship with ε, which can be expressed in Equation 7 (Zhang et al., 2021a):

$$P_i(\varepsilon) \propto \varepsilon^{\alpha_i} \tag{7}$$

In this equation, α_i represents the Lipschitz-Hölder exponent or singularity strength, indicating the density of data distribution. A smaller α_i value implies a higher degree of data variation or heterogeneity, while a larger α_i value corresponds to greater regularity or uniformity in the data (i.e., higher regularity or orderliness).

It's possible that different values of (ε) might share the same singularity strength. This can be represented by Equation 8, which denotes the proportion of the total dataset that is occupied by the sum of segmented datasets with singularity strengths clustered around α within a given (ε) range:

$$N_\alpha(\varepsilon) \propto \varepsilon^{-f(\alpha)} \tag{8}$$

Here, $f(\alpha)$ represents the multifractal spectrum or singularity spectrum. A wider peak in the multifractal spectrum indicates stronger local heterogeneity. A greater right-side skewness reflects greater diversity in singularity exponents, which is associated with sparse pore size distributions. Conversely, greater left-side skewness indicates greater diversity in the smallest singularity exponents, which is linked to higher aggregation probabilities.

The partition function Equation 9 is defined as (Zhang et al., 2022):

$$X(q,\varepsilon) = \sum_{i=1}^{N(\varepsilon)} P_i(\varepsilon)^q \propto \varepsilon^{\tau(q)} \tag{9}$$

Here, q represents the order moment or weighting factor, ranging from -∞ to +∞. When $q > 1$, information from high-density regions (dense areas) is amplified. Conversely, when $q < 1$, information from low-density regions (sparse areas) is amplified. $\tau(q)$ denotes the mass function, which can be expressed by Equation 10:

$$\tau(q) = -\lim_{\varepsilon\to 0}\frac{lgx(q,\varepsilon)}{lg\,\varepsilon} = -\lim_{\varepsilon\to 0}\frac{lg\sum_{i=1}^{N(\varepsilon)}P_i(\varepsilon)^q}{lg\,\varepsilon} \tag{10}$$

Different q values correspond to different generalized fractal dimensions $D(q)$, which can be calculated using Equation 11 as follows (Zhao et al., 2017):

$$D(q) = \begin{cases} \dfrac{\tau(q)}{1-q} = \dfrac{1}{q-1}\dfrac{lg\sum_{i=1}^{N(\varepsilon)}P_i(\varepsilon)^q}{lg\,\varepsilon}, q \neq 1 \\ \dfrac{\sum_{i=1}^{N(\varepsilon)}P_i(\varepsilon)\,lg\,P_i(\varepsilon)}{lg\,\varepsilon}, q = 1 \end{cases} \tag{11}$$

The relationship between the singularity strength $\alpha(q)$, $f(\alpha)$, and $\tau(q)$ corresponding to the order moment q, derived from the Legendre transform, can be expressed by Equations 12, 13 (Liu et al., 2018):

$$\alpha(q) = \frac{d\tau(q)}{dq} \tag{12}$$

$$f(\alpha) = q\alpha(q) - \tau(q) \tag{13}$$

Within the generalized fractal spectrum $q \sim D(q)$, the extracted $D(q)$ values reveal the distribution characteristics of the dataset. In the multifractal spectrum $\alpha \sim f(\alpha)$, extracted values of $\alpha(q), f(\alpha)$, and the spectral width $\Delta\alpha$ provide insight into the dataset's distribution. The spectral width $\Delta\alpha$ can be expressed by Equation 14:

$$\Delta\alpha = \alpha_{max} - \alpha_{min} \tag{14}$$

4 Result

4.1 Mineral characteristics and lithofacies types

Mineralogical analysis, including cast thin sections, SEM with energy-dispersive X-ray spectroscopy (SEM-EDS), and XRD, indicates that quartz and clay minerals are the dominant constituents of the shale samples, averaging 47.26% and 28.56%, respectively. Illite-smectite mixed layers and illite comprise the predominant clay mineral species. Feldspars constitute a significant proportion of the assemblage (0.8%–37.5%, averaging 18.59%), with plagioclase predominating. Carbonate minerals are present in relatively minor amounts (averaging 5.59%), primarily calcite (Figure 2).

Lithofacies, defined by rock characteristics (composition, geochemistry, and sedimentary structures) and depositional environment (He et al., 2024), were classified within the Lianggaoshan Formation using a "four-component, three-end-member" scheme that incorporates TOC, rock fabric, and inorganic mineral composition (Figure 3A) (Feng et al., 2024). Given the limited range of organic matter abundance in the Lianggaoshan Formation (TOC generally <2%), thresholds of 0.6% and 1.5% TOC were selected to delineate organic matter content (Wang et al., 2024; Yin et al., 2024). This classification scheme identified four dominant lithofacies: high-organic matter laminated felsic shale, medium-organic bedded felsic shale, low-organic massive argillaceous siltstone, and massive fine-silt sandstone (Figure 3B).

4.2 Geochemical characteristics

Organic geochemical analysis of Lianggaoshan Formation shales in the northeastern Sichuan Basin reveals favorable hydrocarbon generation potential. The relationship between TOC content and hydrocarbon generation potential (S_1 + S_2) reveals the varying hydrocarbon-generating capacities of different lithofacies (Xue et al., 2024). TOC values range from 0.15% to 2.95% (average 1.09%), indicating overall promising hydrocarbon generation potential. High-organic laminated felsic shales exhibit higher TOC and stronger hydrocarbon generation capacity, largely concentrated within the "Good" range, suggesting significant potential (Figure 4A). Conversely, medium-organic bedded felsic shale, low-organic massive argillaceous siltstone, and massive fine-silt sandstone exhibit a comparatively lower hydrocarbon-generating capacity, falling within thre "Poor" to "Fair" egions. The relationship between hydrogen index (HI) and pyrolytic peak temperature (T_{max}) further clarifies the type and maturity of organic matter in these shales (Hu et al., 2024a). The T_{max} of the shales in study area ranges from 336°C to 494°C, with an average of 468.15°C, indicating that the organic matter is mature to highly mature. R_o values (1.06%–1.68%, average 1.46%) corroborate these findings, confirming the high maturity. The organic matter primarily comprises Type II_1 and Type II_2 kerogen, with a high proportion (67%–78%) of sapropelic organic matter (Figure 4B), further supporting significant oil generation potential.

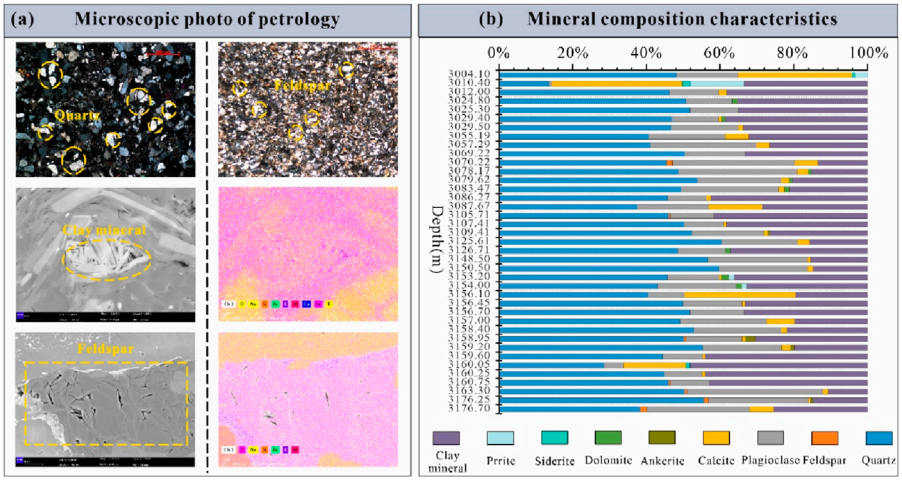

FIGURE 2
Mineralogical characteristics of the Lianggaoshan formation shales. **(A)** Microscopic and scanning electron microscopy observations of mineral microstructures; **(B)** Shale mineral composition.

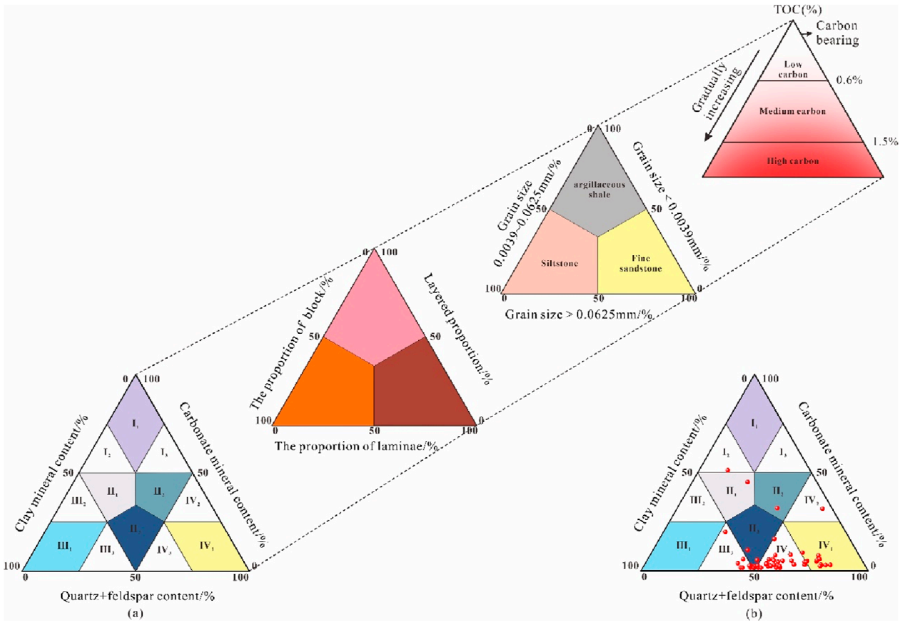

FIGURE 3
Lithofacies classification of Lianggaoshan formation shale. **(A)** lithofacies division scheme; **(B)** The results of lithofacies division in the study area.

4.3 Pore type

Analysis of Jurassic Lianggaoshan Formation shales in the northeastern Sichuan Basin reveals significant lithofacies-dependent variations in pore type and development (Wang et al., 2024). Based on SEM observations and the shale pore classification scheme proposed by Loucks et al. (2012), the main pore types in the study area identified include clay mineral interparticle pores, organic pores, quartz dissolution pores, intergranular pores, pyrite interparticle pores, and microfractures. High-organic laminated felsic shales exhibit abundant organic pores, predominantly irregular in shape and ranging from 100 to 500 nm in size (Figure 5A). Inorganic porosity is represented by intragranular dissolution pores and pyrite interparticle pores. Additionally, intergranular pores formed by mineral edge dissolution are also relatively well developed, with pore sizes generally exceeding 1 μm. This lithofacies exhibits a diverse array of pore types, with localized areas displaying honeycomb-like organic pores, indicating a high potential for reservoir space development (Figures 5B, C).

Medium-organic bedded felsic shale is characterized by intergranular pores between inorganic rigid grains as the main pore type. While organic pores are also present, their volume proportion

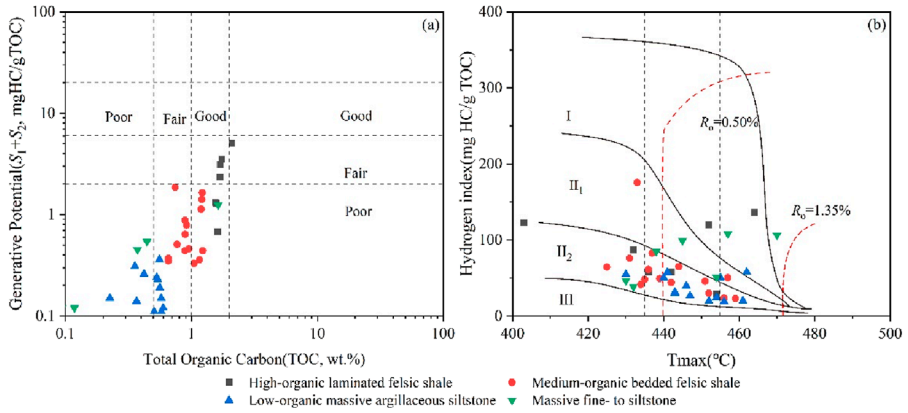

FIGURE 4
Hydrocarbon generation potential of shales of the Jurassic Lianggaoshan formation in the northeastern Sichuan Basin. **(A)** Relationship between hydrocarbon generation potential (S_1+S_2) and TOC; **(B)** Classification of organic matter types in the Lianggaoshan Formation shales.

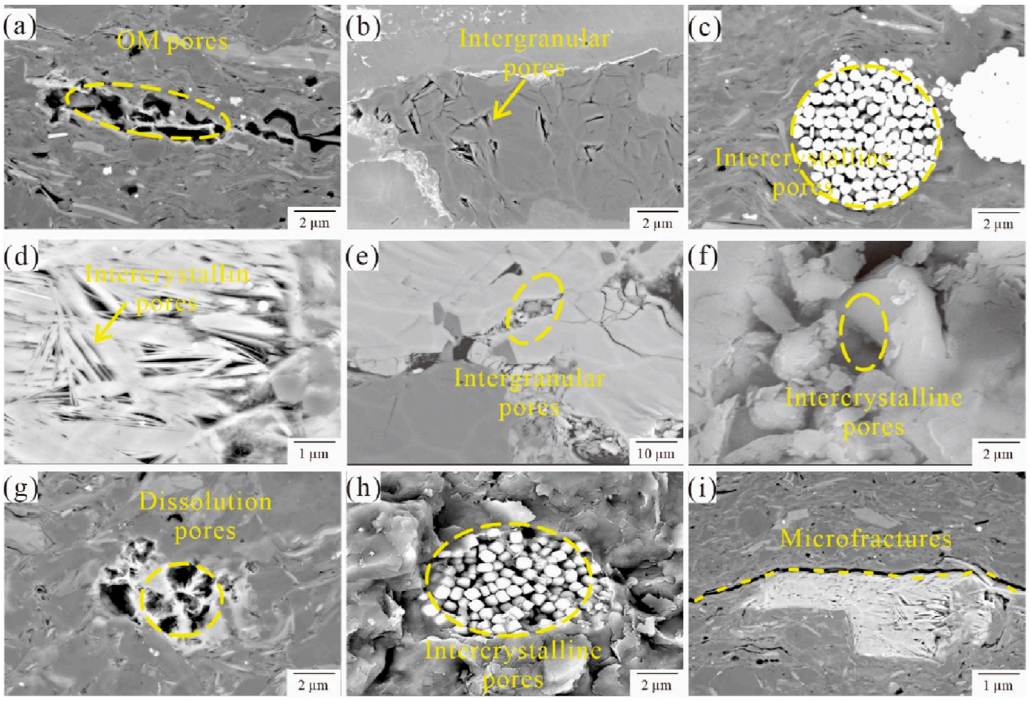

FIGURE 5
Different lithofacies pore types of shales of the Jurassic Lianggaoshan formation in the northeastern Sichuan Basin. **(A)** PY1,3115.51m, High-organic laminated felsic shale; **(B)** PA1,2904.92m, High-organic laminated felsic shale; **(C)** DY1,3159.00m, High-organic laminated felsic shale; **(D)** PY1,3114.66m, Medium-organic bedded felsic shale; **(E)** PY1,3091.73m, Medium-organic bedded felsic shale; **(F)** PA1,3007.5m, Low-organic massive argillaceous siltstone; **(G)** PA1,3008.9m, Low-organic massive argillaceous siltstone; **(H)** PY1,3115.51m, massive fine-silt sandstone; **(I)** PA1,2904.02m, massive fine-silt sandstone.

is relatively low, mainly concentrated within dissolution pores on the surface of feldspars (Figure 5D). Intergranular pores are well developed in this lithofacies, and quartz dissolution pores also constitute a significant proportion, demonstrating a certain degree of storage capacity (Figure 5E).

Low-organic massive argillaceous siltstone and massive fine-silt sandstone exhibit a relatively simple pore type. Poorly developed organic pores, primarily irregular shapes filling interparticle spaces between quartz grains and clay minerals, are observed (Figures 5F, G). Inorganic pore development is limited in this lithofacies, with relatively few pyrite interparticle pores and microfractures (Figures 5H, I). Consequently, these lithofacies exhibit limited reservoir potential.

4.4 Pore structure characteristics of different lithofacies shales

CO_2GA, LTN$_2$A and MIP experiments were conducted to characterize the pore morphology of different lithofacies within the Jurassic Lianggaoshan Formation shales of the northeast Sichuan Basin. High-organic laminated felsic shale exhibits a distinct co-existence of micropores, mesopores, and macropores (Figures 6A–C). CO_2 adsorption experiments demonstrate well-developed mesopores, primarily exhibiting irregular shapes below 100 nm (Figure 6A). These micropores often exhibit fine, crack-like, or intergranular forms. N_2 adsorption experiments further revealed mesopores, predominantly exhibiting ink-bottle-like and parallel plate-like pores morphologies (Figure 6B). Hysteresis in the adsorption-desorption isotherms indicates pore connectivity and complex morphology. MIP porosimetry revealed well-developed macropores and microfractures, exhibiting predominantly slit-shaped and near-circular morphologies in the nanometer to micrometer rang (Figure 6C).

Medium-organic bedded felsic shale exhibits a simpler pore morphology (Figures 6D–F). CO_2 adsorption experiments indicate that the micropores primarily comprised irregular intergranular pore spaces (Figure 6D), but their development was less pronounced than in high-organic laminated felsic shale. N_2 adsorption experiments showed that mesopores were mainly slit-shaped and plate-shaped (Figure 6E), but their hysteresis loop characteristics are less pronounced compared to high-organic matter lithofacies, indicating lower complexity of these mesopores. MIP experiments reveal the limited development of macropores and microfractures, with the pore morphology primarily characterized by simple intergranular pores (Figure 6F), resulting in a relatively simple overall pore structure and limited reservoir potential.

Low-organic matter massive argillaceous siltstone exhibits a more simplified and limited pore morphology (Figures 6G–I). CO_2 adsorption experiments show limited micropore development, with the pore morphology primarily characterized by a small number of irregular and tiny intergranular pores (Figure 6G). N_2 adsorption experiments reveal a limited number of mesopores, with the pore morphology primarily characterized by ink-bottle-like and slit-shaped (Figure 6H). The hysteresis loop characteristics suggest poor connectivity of these pores. MIP experiments indicated very limited macropore and microfracture development (Figure 6I), with the pore structure consisting primarily of simple linear or point-like features, thus limiting the storage capacity of this lithofacies.

Massive fine-silt sandstone exhibits a slightly improved pore morphology (Figures 6J–L). CO_2 adsorption experiments revealed a limited development of micropores, primarily exhibiting irregular intergranular spaces (Figure 6J). N_2 adsorption experiments show a more developed mesoporous and macroporous morphology, with hysteresis loop characteristics suggesting that these pores are mainly wedge-shaped, ink-bottle-like, and plate-shaped (Figure 6K). MIP experiments further indicated relatively well-developed macropores and microfractures (Figure 6L), characterized by near-circular or linear morphologies and a wide pore size distribution.

4.5 Pore size distribution characteristics of different lithofacies shales

By integrating low-temperature gas adsorption (CO_2 and N_2) with high-pressure mercury intrusion data, the pore volume distribution characteristics of different lithofacies of the Jurassic Lianggaoshan Formation shales in Northeast Sichuan Basin were systematically analyzed. Analysis of pore volume distribution in high-organic laminated felsic shale revealed a significant dominance of mesopores (Figures 7A, B). The pore size distribution peaked between 10 and 100 nm, with mesopores comprising 68.3%, micropores 28.7%, and macropores only 3.0% of the total pore volume. This indicates that mesopores constitute the primary reservoir space within this lithofacies.

The pore volume distribution of medium-organic bedded felsic shale similarly exhibits a predominance of mesopores (Figures 7D, E). The pore size distribution peak between 10 nm and 50 nm, with mesopores comprising 64.2%, micropores 32.5%, and macropores only 3.3% of the total pore volume. Compared to high-organic matter laminated felsic shale, the relative proportion of mesopores is slightly lower, but they still constitute the primary reservoir space.

The pore volume distribution of low-organic matter massive argillaceous siltstone is dominated by micropores, with the pore size distribution primarily concentrated within the range of 1 nm–10 nm, with micropores accounting for 58.7% of the total pore volume, mesopores contributing 35.4%, and macropores accounting for only 5.9% (Figures 7G, H). This indicates that micropores comprise the primary reservoir space in this lithofacies.

Massive fine-silt sandstone exhibits a more balanced pore size distribution, concentrated between 10 and 50 nm (Figures 7J, K). Mesopores comprise 59.8%, micropores 29.1%, and macropores 11.1% of the total pore volume. Compared to other lithofacies, this lithofacies shows a slightly higher proportion of macropores; however, mesopores remain the primary reservoir space.

By converting the NMR T_2 spectra to specific pore sizes (Figures 7C, F, I, L), the results indicate that the nuclear magnetic conversion pores are consistent with the pore size distribution morphology obtained from experiments. Furthermore, after conversion, the T_2 spectral distribution peaks of the four rock cores show a high degree of overlap with the peaks of the combined pore size distributions obtained from CO_2 adsorption, low-temperature N_2 adsorption, and MIP.

4.6 Multifractal characteristics of different lithofacies shales

Multifractal theory, through D(q) and f(α) indices, quantifies the spatial distribution and heterogeneity of pore structures, clarifying pore complexity and heterogeneity at various microscopic scales, which is crucial for predicting hydrocarbon accumulation space and flow paths. By analyzing the multifractal characteristics of high-organic-content lamellar feldspathic shale, medium-organic-content lamellar feldspathic shale, low-organic-content blocky argillaceous siltstone, and silty sandstone from the Jurassic Lianggaoshan Formation in Northeast Sichuan, we uncover the complexity and heterogeneity of pore structures across different

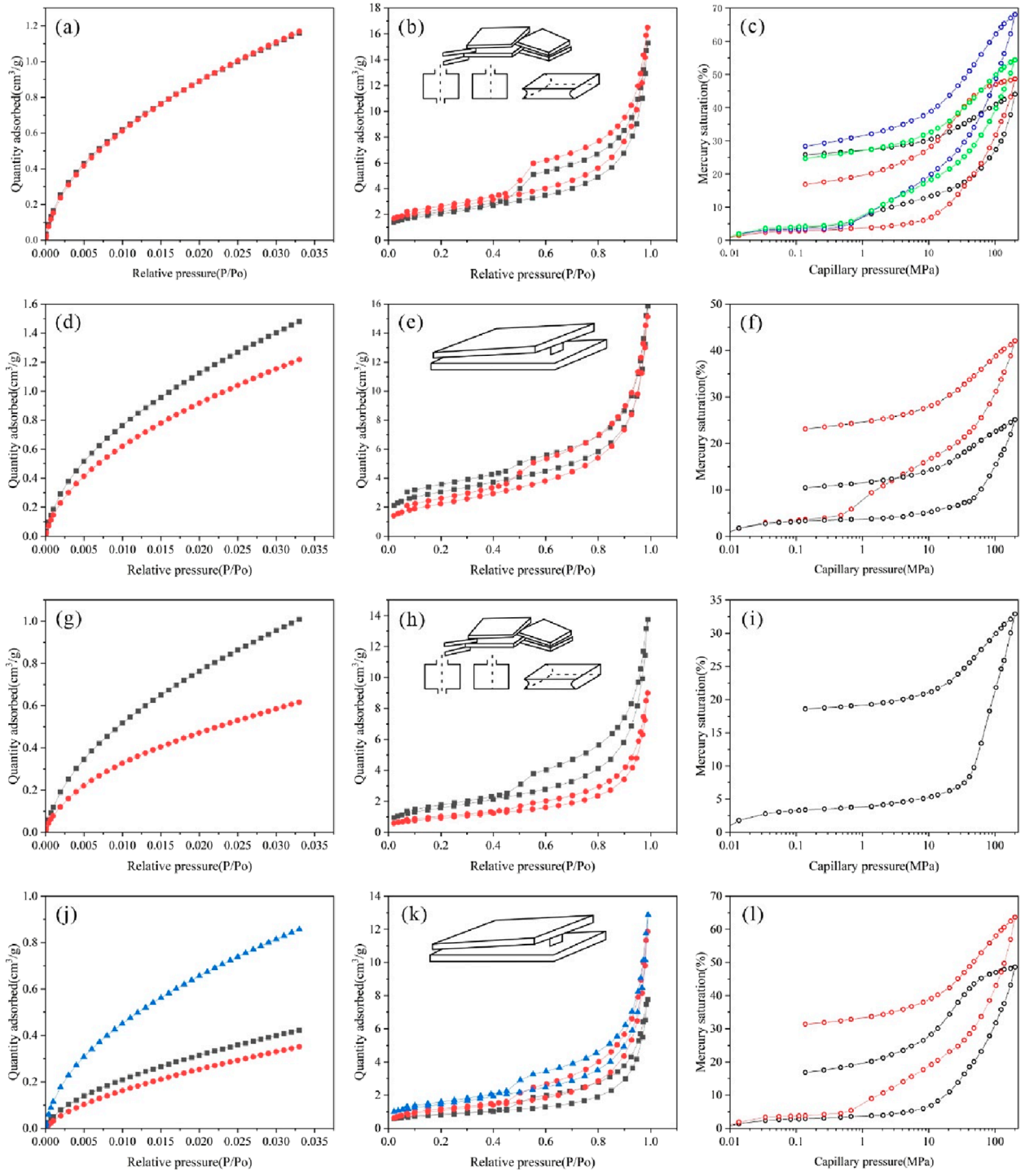

FIGURE 6
CO_2 adsorption, N_2 adsorption-desorption, and high-pressure mercury intrusion-extrusion curves for different shales lithofacies of the Jurassic Lianggaoshan formation shales in the northeastern Sichuan Basin. **(A–C)** High-organic matter laminated felsic shale; **(D–F)** Medium-organic bedded felsic shale; **(G–I)** Low-organic matter massive argillaceous siltstone; **(J–L)** massive fine-silt sandstone.

lithofacies (Figure 8). The pore size distribution and multifractal analysis of the high-organic-content lamellar feldspathic shale (Figures 8A–C) indicate that its generalized fractal dimension D(q) decreases with increasing q. The D(q) curve in Figure 8B shows thatΔD increases with q, reflecting significant heterogeneity in this lithofacies; the multifractal spectrum f(α) in Figure 8C shows a broad distribution of Δα and αmax, further indicating that this heterogeneity is concentrated in low-probability regions. Similarly, the medium-organic-content lamellar feldspathic shale (Figures 8D–F) shows high heterogeneity, albeit slightly lower

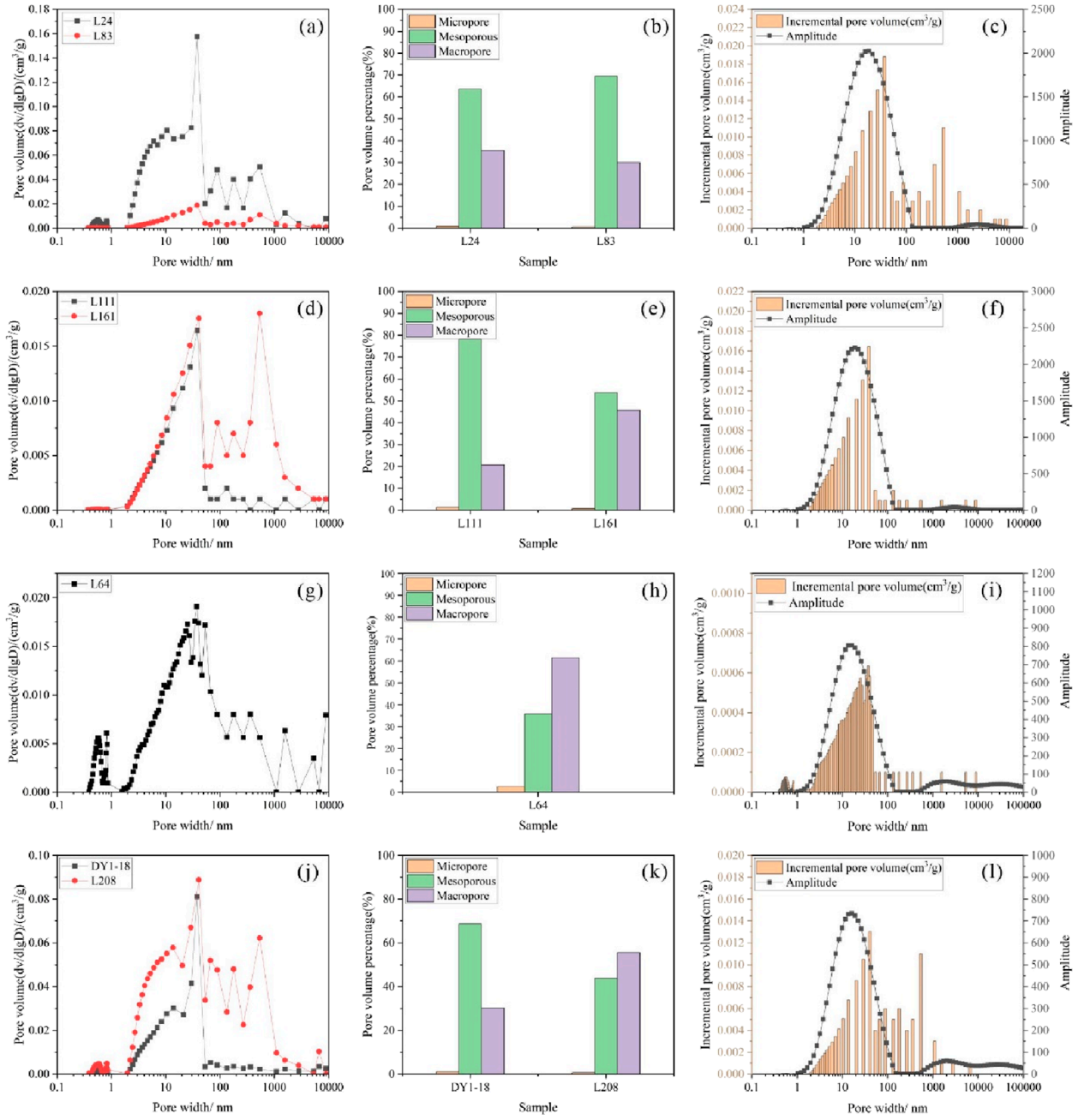

FIGURE 7
Pore size distribution curves, pore volume fraction histograms, and corresponding pore size conversion relationships from NMR T_2 spectra for different lithofacies of the Jurassic Lianggaoshan formation shales in the northeastern Sichuan Basin. **(A–C)** High-organic matter laminated felsic shale; **(D–F)** Medium-organic bedded felsic shale; **(G–I)** Low-organic matter massive argillaceous siltstone; **(J–L)** Massive fine-silt sandstone.

than that of the high-organic-content lithofacies, and its f(α) analysis suggests that the heterogeneity mainly arises from low-probability regions. The multifractal characteristics of the low-organic-content blocky argillaceous siltstone (Figures 8G–I) and the silty sandstone (Figures 8J–L) reveal lower heterogeneity. The D(q) curve of the low-organic-content lithofacies exhibits a smaller increment, indicating relatively homogeneous pore structures; its f(α) analysis further confirms that the heterogeneity is concentrated in medium-probability regions.

5 Discussion

5.1 Influencing factors of shale pore structure development

In high-organic matter laminated felsic shale, macropore pore volume exhibits a positive correlation with TOC content (R^2 = 0.59) (Figures 9A), suggesting that higher organic matter content promotes macropore development, consistent with the

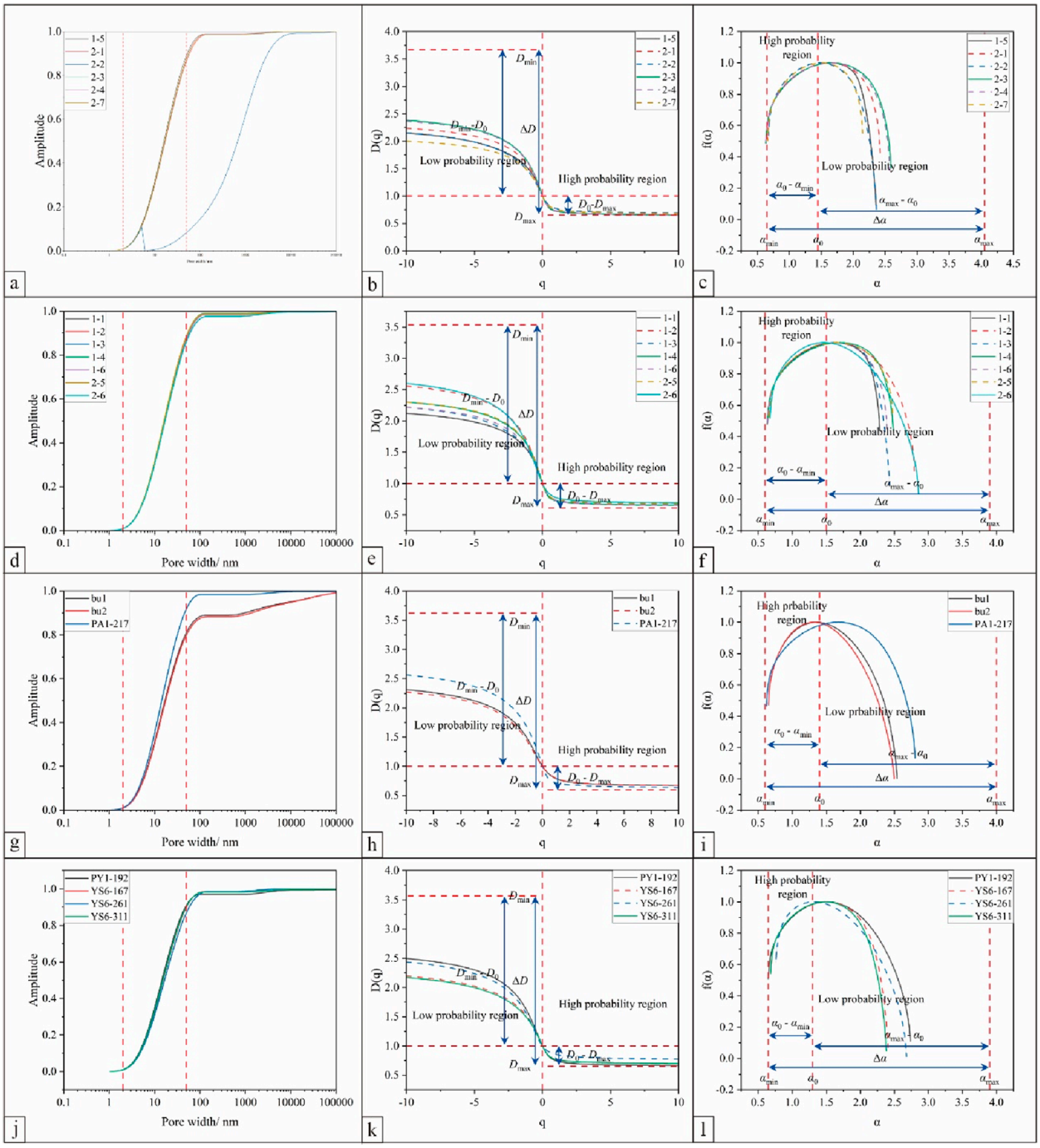

FIGURE 8
Normalized cumulative curves of T_2 spectra, multifractal spectrum functions, and generalized fractal dimension spectra for different lithofacies of the Jurassic Lianggaoshan formation shales in the northeastern Sichuan Basin. **(A–C)** High-organic matter laminated felsic shale; **(D–F)** Medium-organic bedded felsic shale; **(G–I)** Low-organic matter massive argillaceous siltstone; **(J–L)** Massive fine-silt sandstone.

hydrocarbon generation process during organic matter thermal evolution (Hu et al., 2024b). This observation aligns with findings in other basins, such as the Bakken Formation, where high TOC content also correlates with macropore development, facilitating oil accumulation (Jiang et al., 2023a; Liu et al., 2024). Meanwhile, quartz content positively influences the development of meso- and micropores (R^2 = 0.71, R^2 = 0.32). Similar trends have been reported by Su et al. (2023) in the Permian Basin, where quartz enrichment enhances pore connectivity and supports hydrocarbon migration. Medium-organic bedded felsic shale shows a negative correlation between micro- and mesoporous volumes and TOC content (R^2 = −0.13, R^2 = −0.27), indicating that the development of micropores and mesopores is restricted under moderate organic matter content, potentially the generation of residual asphalt

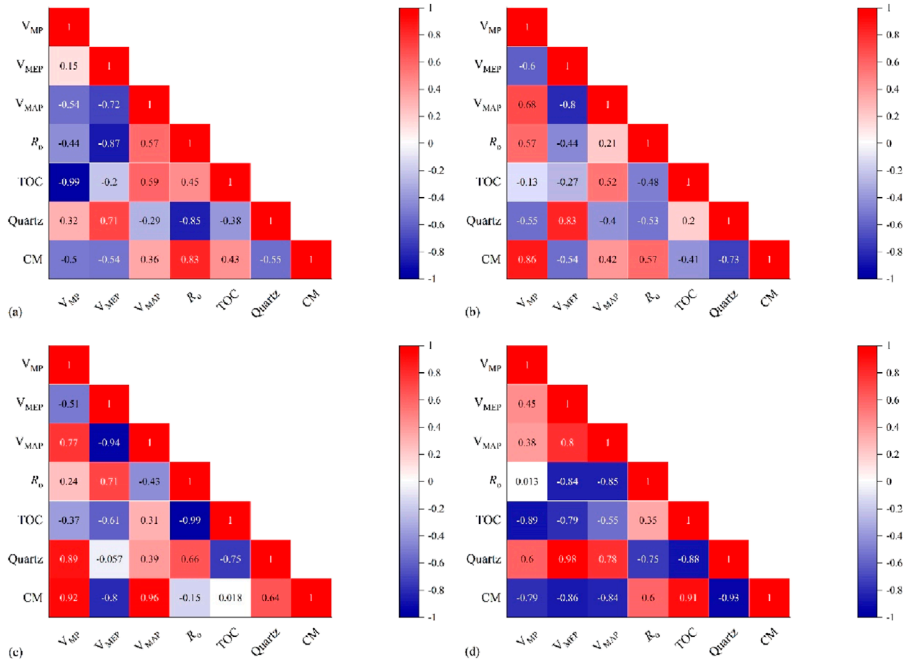

FIGURE 9
Relationship between TOC and mineral composition content and pore structure for shales of the Jurassic Lianggaoshan formation in the northeastern Sichuan Basin. **(A)** High-organic matter laminated felsic shale; **(B)** Medium-organic bedded felsic shale; **(C)** Low-organic massive argillaceous siltstone; **(D)** Massive fine-silt sandstone. Abbreviations: CM = clay minerals.

by the organic matter that blockage the pore space (Guo et al., 2020). Quartz content still promotes mesoporous formation (R^2 = 0.83), while clay minerals also exhibit a tendency to promote pore development. Micro- and macropores show positive correlations with clay mineral content, respectively, indicating that pore structure development in this lithofacies is also significantly influenced by clay minerals (Figure 9B). Despite a positive correlation between macropore volume and TOC content in low-organic matter massive argillaceous siltstone (R^2 = 0.31), suggesting some promotion of macropore development by organic matter, the negative correlation between micro- and mesoporous volumes and TOC content (R^2 = −0.37, R^2 = −0.61) reflects the inhibition of smaller pore space development in low-organic matter shales. Additionally, quartz content exhibits a degree of negative correlation with mesoporous volume in this lithofacies (R^2 = −0.057), suggesting that an increase in quartz content might lead to a reduction in pore space, particularly mesopores. The positive correlation of clay minerals (R^2 = 0.96) further confirms their positive impact on pore development (Figure 9C). In contrast to other lithofacies, micropore, mesopore and macropore volumes in massive fine-silt sandstone exhibit a negative correlation with TOC content (Figure 9D), indicating that an increase in TOC content might lead to a decrease in pore volume. Simultaneously, quartz content exhibits a significant positive impact on the formation of meso- and macropores (R^2 = 0.98), consistent with the trend observed in high-organic matter shales.

In summary, the development extent of pore structures in different lithofacies of shales in the study area is closely related to TOC content, quartz, and clay mineral content. TOC content generally exhibits a positive correlation with the development of micro- and mesopores, although its increase may inhibit pore development in certain lithofacies. Quartz content generally contributes to the formation of meso- and macropores, while an increase in clay mineral content leads to the formation of numerous intercrystalline pores, also playing a positive role in shale pore development.

5.2 Influencing factors of shale multifractal dimension

The diverse composition of shales is a key factor driving the variability in pore structures. Compared to conventional reservoirs, shale reservoirs not only exhibit complex mineral assemblages but also contain organic matter and abundant organic pores (Wang et al., 2023). The application of multifractal theory provides a quantitative evaluation of pore structure heterogeneity across various lithofacies, addressing a notable gap in current research. For instance, Zhang et al. (2024a) primarily investigated the effects of TOC and quartz content but did not incorporate multifractal metrics such as ΔD and Δα, which are crucial for understanding heterogeneity at multiple scales. In high-organic matter laminated felsic shale, ΔD shows a significant positive correlation with quartz content (R^2 = 0.55), while clay mineral content exhibits a negative correlation (R^2 = −0.37) (Figure 10A). This suggests that quartz enrichment enhances shale compaction resistance, reducing pore structure heterogeneity, whereas clay minerals contribute to increased heterogeneity due to compaction. The correlation between TOC content and ΔD and Δα is weak, indicating a limited influence

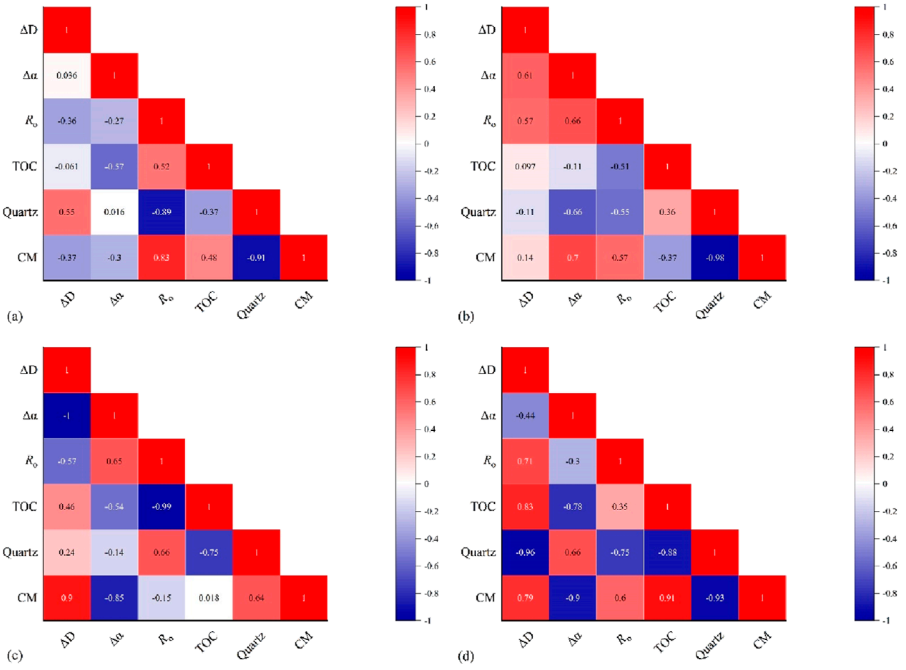

FIGURE 10
Relationship between TOC and mineral composition content and multifractal dimension for shales of the Jurassic Lianggaoshan formation in the northeastern Sichuan Basin. **(A)** High-organic matter laminated felsic shale; **(B)** Medium-organic bedded felsic shale; **(C)** Low-organic massive argillaceous siltstone; **(D)** Massive fine-silt sandstone. Abbreviations: CM = clay minerals.

of TOC on pore heterogeneity in this lithofacies. In medium-organic bedded felsic shale, ΔD shows a weak correlation with TOC content, while a positive correlation with clay mineral content is observed (R^2 = 0.14) (Figure 10B). This indicates that clay minerals play a more prominent role in enhancing pore heterogeneity in this lithofacies, while quartz, although exhibiting a certain degree of heterogeneity reduction, has a relatively minor impact. In low-organic matter massive argillaceous siltstone, quartz content is positively correlated with ΔD (R^2 = 0.24) (Figure 10C), indicating that quartz continues to contribute to pore structure homogeneity even under low-organic matter conditions. However, the negative correlation between clay mineral content and ΔD and Δα (R^2 = −0.85 and −0.9) suggests that clay minerals are more prone to induce pore structure complexity and enhanced heterogeneity in low-organic matter shales. Massive fine-silt sandstone exhibits a strong positive correlation between TOC content and ΔD (R^2 = 0.83) (Figure 10D), reflecting that organic matter enrichment can lead to a significant increase in pore heterogeneity. The negative correlation between quartz and ΔD (R^2 = −0.96) suggests that quartz helps maintain pore structure homogeneity in this lithofacies, while clay minerals continue to enhance pore structure heterogeneity.

In summary, the controlling mechanisms of quartz and clay minerals on pore structure heterogeneity in different lithofacies exhibit significant differences. An increase in quartz content typically contributes to reduced heterogeneity, while an increase in clay mineral content often leads to enhanced heterogeneity. The influence of TOC varies among different lithofacies, with a particularly prominent effect in massive fine-silt sandstone.

5.3 The relationship between pore structure and pore multifractal characteristics and its geological significance

Figure 11A reveals that the ΔD values for micropores are concentrated between 1.3 and 1.5, with a smaller pore volume, suggesting a relatively uniform micropore structure and low heterogeneity. The ΔD values for mesopores exhibit a wider range, reaching 1.5 to 1.9, with a larger variation in pore volume, reflecting a more complex mesoporous structure and stronger heterogeneity. The ΔD values for macropores are relatively scattered, with larger pore volumes, but the correlation between ΔD and pore volume is not pronounced, implying that the formation of macropores is influenced by multiple geological factors, resulting in a higher level of structural complexity and heterogeneity. Figure 11B illustrates the relationship between pore volume and roughness Δα. The Δα values for micropores are smaller, concentrated between 0.5 and 0.6, indicating smooth and uniform micropore surfaces. The Δα values for mesopores and macropores have a wider distribution, particularly for mesopores, which can reach 1.0, reflecting a rougher surface and higher heterogeneity in mesopores and macropores (Zhang et al., 2021b).

In high-organic matter laminated felsic shale, micropores exhibit lower fractal dimensions (ΔD) and roughness (Δα), indicating a simpler and more uniform pore structure. This observation aligns with the development characteristics of organic pores in high-organic matter shales. Micropores primarily form during the thermal evolution of organic matter, resulting in regular pore

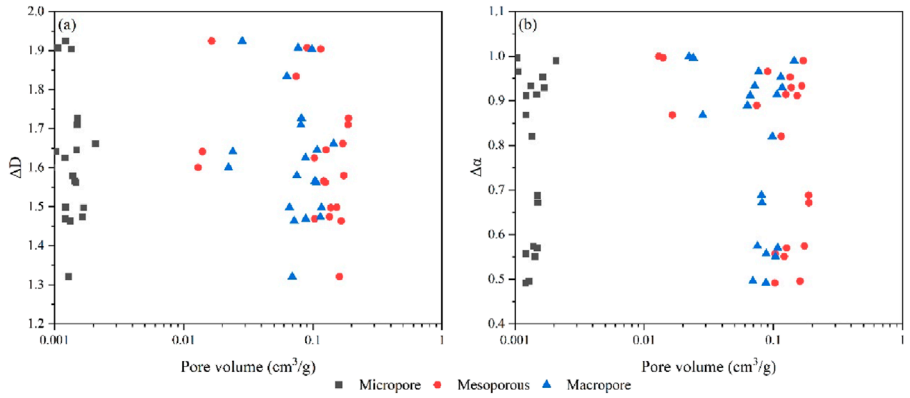

FIGURE 11
Relationship between multifractal dimension parameters and pore structure in shales of the Jurassic Lianggaoshan formation in the northeastern Sichuan Basin. **(A)** Relationship between ΔD values and pore volume; **(B)** Relationship between Δα values and pore volume.

morphology, stable structure, and low heterogeneity (Zhu et al., 2023; Liang et al., 2024). These micropores play a crucial role in shale oil enrichment by providing stable reservoir space. In medium-organic bedded felsic shale, mesopores exhibit higher ΔD and Δα values, reflecting a complex and heterogeneous pore structure in this lithofacies. Mesopores dominate this lithofacies, controlled by the enrichment and distribution of siliceous minerals. High silica content contributes to the formation of complex pore networks, increasing pore connectivity and complexity, thereby enhancing shale oil mobility. However, this complexity introduces uncertainty in exploration and development. Macropores in low-organic matter massive argillaceous siltstone exhibit high ΔD values and a wide distribution of Δα values, indicating a high degree of pore structure heterogeneity. Macropores are predominantly composed of interlayer and intergranular pores in clay minerals. Clay minerals are prone to deformation during diagenesis and compaction, leading to complex macropore structures and increased surface roughness (Jiang et al., 2023b; Liang et al., 2024). While the presence of macropores provides pathways for fluid flow, their high heterogeneity may restrict effective fluid migration and recovery (Chang et al., 2024b; Chen et al., 2024b). In massive fine-silt sandstone, the ΔD and Δα values of all pore types exhibit significant variations, reflecting an exceptionally complex and heterogeneous pore structure in this lithofacies. This high heterogeneity is likely controlled by the combined effect of quartz and clay minerals in the rock, particularly when quartz content is high, complex pore networks develop, while the plastic deformation of clay minerals further exacerbates surface roughness and structural irregularity.

Therefore, the pore structures and multifractal characteristics of different lithofacies within the Lianggaoshan Formation display significant variations, providing an in-depth understanding of reservoir flow capacity and hydrocarbon enrichment potential. Compared to conventional porosity-permeability models used in previous studies, the application of multifractal dimensions provides a more nuanced characterization of pore heterogeneity and its influence on reservoir quality. The micropore structure of high-organic-matter shale is simple and uniform; this low heterogeneity and narrow pore size distribution favor the accumulation and retention of shale oil. In contrast, the mesopore structure of medium-organic-matter lithofacies is relatively complex. Although its pore structure is conducive to hydrocarbon accumulation, its high heterogeneity poses challenges to development, such as uneven flow paths and increased seepage resistance. Conversely, the low-organic-matter lithofacies exhibits prominent macropore structures and high heterogeneity, which may reduce effective hydrocarbon recovery rates. Additionally, the pore structure of blocky fine-silty sandstone lithofacies shows extreme complexity and heterogeneity, reflecting the influence of quartz-clay mineral interactions on pore development. Multifractal analysis, using generalized fractal dimensions D(q) and multifractal spectra f(α), provides quantitative insights into the pore heterogeneity of different lithofacies and their distribution across probability regions, enabling us to reveal shale reservoir structural characteristics at a microscopic scale. This analytical approach offers scientific support for predicting reservoir flow paths and optimizing "sweet spot" zones, thereby providing critical backing for the exploration and development of shale oil resources within the Lianggaoshan Formation in the Sichuan Basin.

6 Conclusion

(1) Significant variations in pore structure characterize the different Lianggaoshan Formation shale lithofacies. High-organic laminated felsic shales are dominated by mesopores, exhibiting a uniform pore structure conducive to shale oil accumulation and preservation. Medium-organic bedded felsic shales comprise both meso- and micropores, resulting in a complex and heterogeneous pore network. Low-organic massive argillaceous siltstones exhibit limited macroporosity and a complex, highly heterogeneous pore structure that may impede effective hydrocarbon migration and recovery. Finally, massive fine-silt sandstones display a complex macroporous structure with multiple pore types, suggesting a relatively poor reservoir capacity.

(2) Analysis indicates an inverse relationship between quartz content and shale pore structure heterogeneity; increasing quartz content reduces heterogeneity, while increasing clay mineral content enhances it. High-organic shales exhibit

a simple, uniform mesoporous structure ideal for shale oil enrichment. Medium-organic lithofacies display complex mesoporosity, but this is accompanied by high heterogeneity, posing challenges for exploration and development. Low-organic lithofacies exhibit a complex and highly heterogeneous macroporous structure, potentially impairing hydrocarbon recovery efficiency.

(3) This research unveils the differences in pore structure and multifractal characteristics among different lithofacies of shales, which exert a significant impact on shale oil enrichment and mobility. High-organic matter shales provide favorable reservoir space, while the mesoporous structure in moderate-organic matter lithofacies facilitates oil and gas accumulation. Conversely, the pore structure in low-organic matter lithofacies may limit shale oil recovery efficiency. These findings offer a scientific basis for the exploration and development of shale oil resources in the Lianggaoshan Formation, guiding the optimization of "sweet spot" selection.

Data availability statement

The raw data supporting the conclusions of this article will be made available by the authors, without undue reservation.

Author contributions

JW: Data curation, Project administration, Writing–review and editing. HS: Conceptualization, Methodology, Project administration, Writing–review and editing. YZ: Conceptualization, Methodology, Writing–original draft, Writing–review and editing. ZJ: Funding acquisition, Project administration, Writing–review and editing. BG: Investigation, Supervision, Writing–original draft. LL: Methodology, Writing–original draft. HP: Methodology, Writing–review and editing. HW: Methodology, Writing–review and editing. XL: Methodology, Writing–original draft. HQ: Conceptualization, Methodology, Writing–original draft. XH: Methodology, Visualization, Writing–original draft. CZ: Visualization, Writing–original draft.

Funding

The author(s) declare that financial support was received for the research, authorship, and/or publication of this article. This work is financially supported by National Natural Science Foundation of China (42272137) and PetroChina Science and Technology Project (2023ZZ15YJ01). The authors declare that this study received funding from PetroChina. The funder was not involved in the study design, collection, analysis, interpretation of data, the writing of this article, or the decision to submit it for publication.

Conflict of interest

Authors JW, HS, BG, LL, HP, HW, XL, and HQ were employed by PetroChina Daqing Oilfield Exploration and Development Research Institute.

The remaining authors declare that the research was conducted in the absence of any commercial or financial relationships that could be construed as a potential conflict of interest.

Generative AI statement

The author(s) declare that no Generative AI was used in the creation of this manuscript.

Publisher's note

References

Bal, A., Misra, S., Mukherjee, M., Dutta, T. K., Sen, D., Patra, A., et al. (2023). Concurrent influence of geological parameters on the integrated nano-pore structure and discretized pore families of the petroliferous Cambay shale assessed through multivariate dependence measure. *Front. Earth Sci.* 11. doi:10.3389/feart.2023.1157122

Cai, G., Gu, Y., Xiong, X., Li, X., Sun, X., Ni, J., et al. (2023). Reservoir characteristics and pore fluid evaluation of Shan 23 Submember transitional shale, eastern Ordos Basin, China: insights from NMR experiments. *Front. Earth Sci.* 10. doi:10.3389/feart.2022.1061211

Cao, Y., Jin, Z. J., Zhu, R. K., and Liu, K. Q. (2024). Pore systems and their correlation with oil enrichment in various lithofacies of saline lacustrine shale strata. *Int. J. Coal Geol.* 282, 104444. doi:10.1016/j.coal.2024.104444

Chang, J. Q., Fan, X. D., Jiang, Z. X., Wang, X. M., Chen, L., Li, J. T., et al. (2022). Differential impact of clay minerals and organic matter on pore structure and its fractal characteristics of marine and continental shales in China. *Appl. Clay Sci.* 216, 106334. doi:10.1016/j.clay.2021.106334

Chang, J. Q., Jiang, Z. X., Jin, Z. H., Gao, Z. Y., Zhang, Y. H., Chen, Z. X., et al. (2024a). Complementary laboratory experiments and molecular dynamics simulation method to investigate the mobility of shale oil: the Permian Fengcheng Formation in the Mahu Sag, Junggar Basin. *Mar. Petroleum Geol.* 167, 106974. doi:10.1016/j.marpetgeo.2024.106974

Chang, X., Lin, S. S., Yang, C. H., Wang, K., Liu, S. M., and Guo, Y. T. (2024b). A critical review of ScCO2-enhanced gas recovery and geologic storage in shale reservoirs. *Gas Sci. Eng.* 125, 205317. doi:10.1016/j.jgsce.2024.205317

Chen, S., Wang, X. J., Li, X. Y., Sui, J. K., Yang, Y. D., Yang, Q., et al. (2024a). Geophysical prediction technology for sweet spots of continental shale oil: a case study of the Lianggaoshan Formation, Sichuan Basin, China. *Fuel* 365, 131146. doi:10.1016/j.fuel.2024.131146

Chen, S. Y., Yang, Y. Q., Wang, X. J., Qiu, L. W., Hu, Y. L., Wu, C. J., et al. (2024b). Genesis mechanism of laumontite cement and its impact on the reservoir of siliciclastic rock: a case study of Jurassic Shaximiao Formation in central Sichuan Basin, China. *Mar. Petroleum Geol.* 165, 106873. doi:10.1016/j.marpetgeo.2024.106873

Chen, Z. X., Wang, L. N., Yang, G., Zhang, B. J., Ying, D. L., Yuan, B. G., et al. (2020). Geological structures and potential petroleum exploration areas in the southwestern Sichuan fold-thrust belt, SW China. *PETROLEUM Explor. Dev.* 47 (4), 699–713. doi:10.1016/s1876-3804(20)60086-6

Cheng, D., Zhang, Z., Hong, H., Zhang, S., Qin, C., Yuan, X., et al. (2023). Sequence structure, sedimentary evolution and their controlling factors of the jurassic Lianggaoshan Formation in the east Sichuan Basin, SW China. *PETROLEUM Explor. Dev.* 50 (2), 293–305. doi:10.1016/s1876-3804(23)60388-x

Daigle, H., Johnson, A., and Thomas, B. (2014). Determining fractal dimension from nuclear magnetic resonance data in rocks with internal magnetic field gradients. *Geophysics* 79 (6), D425–D431. doi:10.1190/geo2014-0325.1

Dimri, V. P., and Ganguli, S. S. (2019). Fractal theory and its implication for acquisition, processing and interpretation (api) of geophysical investigation: a review. *J. Geol. Soc. India* 93 (2), 142–152. doi:10.1007/s12594-019-1142-8

Fang, R., Jiang, Y., Yang, C., Deng, H., Jiang, C., Hong, H., et al. (2024). Occurrence states and mobility of shale oil in different lithologic assemblages in the Jurassic Lianggaoshan Formation, Sichuan Basin. *Oil and Gas Geol.* 45 (3), 752–769. doi:10.11743/ogg20240313

Feng, Y. L., Yang, Z., Jiang, W. Q., Zhang, H., Zhang, T. S., Liu, C., et al. (2024). The influence of mudstone lithofacies sedimentation on the development of shale oil " sweet-spot intervals" within large down-warped lacustrine basins in China. *Mar. Petroleum Geol.* 169, 107063. doi:10.1016/j.marpetgeo.2024.107063

Fleury, M., Gimmi, T., and Mazurek, M. (2022). Porewater content, pore structure and water mobility in clays and shales from NMR methods. *Clays Clay Minerals* 70 (3), 417–437. doi:10.1007/s42860-022-00195-4

Guo, H., Jia, W., He, R., Yu, C., Song, J., and Peng, P. A. (2020). Distinct evolution trends of nanometer-scale pores displayed by the pyrolysis of organic matter-rich lacustrine shales: implications for the pore development mechanisms. *Mar. Petroleum Geol.* 121: 104622. doi:10.1016/j.marpetgeo.2020.104622

Han, Y. H., Jiang, Z. X., Liang, Z. K., Lai, Z. Y., Wu, Y. H., Shi, X. W., et al. (2024). Study on the multifractal characterization and seepage of the shale matrix: a case study of the Longmaxi Formation in southwestern Sichuan Basin, China. *Geoenergy Sci. Eng.* 238, 212924. doi:10.1016/j.geoen.2024.212924

He, W., Bai, X., Meng, Q. A., Li, J., Zhang, D., and Wang, Y. (2022). Accumulation geological characteristics and major discoveries of lacustrine shale oil in Sichuan Basin. *Acta Pet. Sin.* 43 (7), 885–898. doi:10.7623/syxb202207001

He, X. B., Luo, Q., Jiang, Z. X., Qiu, Z. X., Luo, J. C., Li, Y. Y., et al. (2024). Control of complex lithofacies on the shale oil potential in saline lacustrine basins of the Jimsar Sag, NW China: coupling mechanisms and conceptual models. *J. Asian Earth Sci.* 266, 106135. doi:10.1016/j.jseaes.2024.106135

Hu, C. E., Tan, J. Q., Lyu, Q., and Zhang, Y. L. (2024a). Evolution of organic pores in Permian low maturity shales from the Dalong Formation in the Sichuan Basin: insights from a thermal simulation experiment. *Gas Sci. Eng.* 121, 205166. doi:10.1016/j.jgsce.2023.205166

Hu, D., Wei, Z., Liu, R., Wei, X., Chen, F., and Liu, Z. (2021). Enrichment control factors and exploration potential of lacustrine shale oil and gas:A case study of Jurassic in the Fuling area of the Sichuan Basin. *Nat. Gas. Ind.* 41 (8), 1–8. doi:10.1016/j.ngib.2021.08.012

Hu, S. Y., Bai, B., Tao, S. Z., Bian, C. S., Zhang, T. S., Chen, Y. Y., et al. (2022). Heterogeneous geological conditions and differential enrichment of medium and high maturity continental shale oil in China. *PETROLEUM Explor. Dev.* 49 (2), 257–271. doi:10.1016/s1876-3804(22)60022-3

Hu, T., Jiang, F., Pang, X., Liu, Y., Wu, G., Zhou, K., et al. (2024b). Identification and evaluation of shale oil micro-migration and its petroleum geological significance. *PETROLEUM Explor. Dev.* 51 (1), 127–140. doi:10.1016/s1876-3804(24)60010-8

Jiang, F., Huo, L., Chen, D., Cao, L., Zhao, R., Li, Y., et al. (2023a). The controlling factors and prediction model of pore structure in global shale sediments based on random forest machine learning. *Earth-Science Rev.*, 241: 104442. doi:10.1016/j.earscirev.2023.104442

Jiang, F. J., Huo, L. N., Chen, D., Cao, L., Zhao, R. J., Li, Y., et al. (2023b). The controlling factors and prediction model of pore structure in global shale sediments based on random forest machine learning. *Earth-Science Rev.* 241, 104442. doi:10.1016/j.earscirev.2023.104442

Jiang, T., Jin, Z., Liu, G., Hu, Z., Chen, X., Liu, Z., et al. (2022). Investigating the pore structure characteristics and reservoir capacities of lower jurassic continental shale reservoirs in the northeastern Sichuan Basin, China. *Front. Earth Sci.* 10. doi:10.3389/feart.2022.886907

Jouini, M. S., Bouchaala, F., Riahi, M. K., Sassi, M., Abderrahmane, H., and Hjouj, F. (2022). Multifractal analysis of reservoir rock samples using 3D X-ray micro computed tomography images. *IEEE Access* 10, 67898–67909. doi:10.1109/ACCESS.2022.3186476

Li, C. R., Pang, X. Q., Ma, X. H., Wang, E. Z., Hu, T., and Wu, Z. Y. (2021). Hydrocarbon generation and expulsion characteristics of the Lower Cambrian Qiongzhusi shale in the Sichuan Basin, Central China: implications for conventional and unconventional natural gas resource potential. *J. Petroleum Sci. Eng.* 204, 108610. doi:10.1016/j.petrol.2021.108610

Li, Z. Q., Shen, X., Qi, Z. Y., and Hu, R. L. (2018). Study on the pore structure and fractal characteristics of marine and continental shale based on mercury porosimetry, N_2 adsorption and NMR methods. *J. Nat. Gas Sci. Eng.* 53, 12–21. doi:10.1016/j.jngse.2018.02.027

Liang, Z. K., Jiang, Z. X., Xue, Z. X., Tang, X. L., Jiang, Y. Q., Chen, R. H., et al. (2024). Experimental investigation of kerogen structure and heterogeneity during pyrolysis. *Geoenergy Sci. Eng.* 242, 213222. doi:10.1016/j.geoen.2024.213222

Liu, K., Zhang, Z., Safaei-Farouji, M., Fattahi, E., Zhang, H., Liu, B., et al. (2024). Quantifying pore structure heterogeneity of shale samples after solvent extraction following anhydrous and hydrous pyrolysis. *Geoenergy Sci. Eng.* 239: 212978. doi:10.1016/j.geoen.2024.212978

Liu, K. Q., Ostadhassan, M., and Kong, L. Y. (2018). Multifractal characteristics of Longmaxi Shale pore structures by N_2 adsorption: a model comparison. *J. Petroleum Sci. Eng.* 168, 330–341. doi:10.1016/j.petrol.2018.04.072

Loucks, R. G., Reed, R. M., Ruppel, S. C., and Hammes, U. (2012). Spectrum of pore types and networks in mudrocks and a descriptive classification for matrix-related mudrock pores. *Aapg Bull.* 96 (6), 1071–1098. doi:10.1306/08171111061

Pang, P., Han, H., Hu, L. H., Guo, C., Gao, Y., and Xie, Y. H. (2021). The calculations of pore structure parameters from gas adsorption experiments of shales: which models are better? *J. Nat. Gas Sci. Eng.* 94, 104060. doi:10.1016/j.jngse.2021.104060

Rahner, M. S., Halisch, M., Fernandes, C. P., Weller, A., and Dos Santos, V. S. S. (2018). Fractal dimensions of pore spaces in unconventional reservoir rocks using X-ray nano-and micro-computed tomography. *J. Nat. Gas Sci. Eng.* 55, 298–311. doi:10.1016/j.jngse.2018.05.011

Stevens, S. H., Moodhe, K. D., and Kuuskraa, V. A. (2013). China shale gas and shale oil resource evaluation and technical challenges: SPE, SPE-165832-MS

Su, S. Y., Cheng, C., Jiang, Z. X., Shan, X. L., Makeen, Y. M., Gao, Z. Y., et al. (2023). Microscopic pore structure and connectivity of lacustrine shale of the shahejie formation, zhanhua sag, Bohai Bay Basin. *Geoenergy Sci. Eng.* 226, 211800. doi:10.1016/j.geoen.2023.211800

Turlapati, V. Y., Prusty, B. K., and Bakshi, T. (2020). Detailed pore structure study of damodar valley and upper Assam basin shales using fractal analysis. *Energy and Fuels* 34 (11), 14001–14011. doi:10.1021/acs.energyfuels.0c02785

Vafaie, A., Habibnia, B., and Moallemi, S. A. (2015). Experimental investigation of the pore structure characteristics of the Garau gas shale formation in the Lurestan Basin, Iran. *J. Nat. Gas Sci. Eng.* 27, 432–442. doi:10.1016/j.jngse.2015.06.029

Vega, S., and Jouini, M. S. (2015). 2D multifractal analysis and porosity scaling estimation in Lower Cretaceous carbonates. *Geophysics* 80 (6), D575–D586. doi:10.1190/geo2014-0596.1

Wang, B. Y., Liu, B., Sun, G. X., Bai, L. H., Chi, Y. A., Liu, Q., et al. (2021). Evaluation of the shale oil reservoir and the oil enrichment model for the first member of the lucaogou formation, western jimusaer depression, junggar basin, NW China. *Acs Omega* 6 (18), 12081–12098. doi:10.1021/acsomega.1c00756

Wang, G. P., Jin, Z. J., Zhang, Q., Zhu, R. K., Tang, X., Liu, K. Q., et al. (2023). Effects of clay minerals and organic matter on pore evolution of the early mature lacustrine shale in the Ordos Basin, China. *J. Asian Earth Sci.* 246, 105516. doi:10.1016/j.jseaes.2022.105516

Wang, P., Liu, Z., Feng, D., Chen, X., Li, F., Hao, J., et al. (2022a). Microfracture development at Ziliujing lacustrine shale reservoir and its significance for shale-gas enrichment at Fuling in eastern Sichuan Basin, China. *J. Nat. Gas Geoscience* 7 (1), 39–48. doi:10.1016/j.jnggs.2022.03.002

Wang, X., Wang, M., Zhao, C., Yang, X. Y., Jia, Y. D., Wu, R., et al. (2024). Reservoir characteristics and controlling factors of the middle-high maturity multiple lithofacies reservoirs of the Lianggaoshan Formation shale strata in the northeastern Sichuan basin, China. *Mar. Petroleum Geol.* 161, 106692. doi:10.1016/j.marpetgeo.2024.106692

Wang, X., Zhang, G., Tang, W., Wang, D., Wang, K., Liu, J., et al. (2022b). A review of commercial development of continental shale oil in China. *Energy Geosci.* 3 (3), 282–289. doi:10.1016/j.engeos.2022.03.006

Xue, C. Q., Mcbeck, J. A., Lu, H. J., Yan, C. H., Zhong, J. H., Wu, J. G., et al. (2024). Classification of shale lithofacies with minimal data: application to the early Permian shales in the Ordos Basin, China. *J. Asian Earth Sci.* 259, 105901. doi:10.1016/j.jseaes.2023.105901

Yin, C. H., Wang, X. D., Wang, Y. Z., Tian, X. B., Yu, H. S., Wang, Z. G., et al. (2024). Progress and prospects of oil and gas exploration and development of Daqing exploration area in Sichuan Basin. *Petroleum Geol. and Oilfield Dev. Daqing* 43 (4), 59–72. doi:10.19597/J.ISSN.1000-3754.202401048

Yu, T., Liu, H., Liu, B. W., Tang, S., Tang, Y. Z., and Yin, C. (2022). Restoration of karst paleogeomorphology and its significance in petroleum geology-Using the top of the Middle Triassic Leikoupo Formation in the northwestern Sichuan Basin as an example. *J. Petroleum Sci. Eng.* 208, 109638. doi:10.1016/j.petrol.2021.109638

Yuan, M., Zou, C. N., Pan, S. Q., Zhang, G. S., Shi, Q., Xie, L. Y., et al. (2024). Ranking the oil contribution of individual layers in a lacustrine shale oil system based on non-hydrocarbon analysis by FT-ICR MS. *Int. J. Coal Geol.* 288, 104528. doi:10.1016/j.coal.2024.104528

Zhang, J., Han, D., Lin, W., Wang, C., Wang, J., Xiao, X., et al. (2024a). Pore structure and fractal characteristics of coal-bearing cretaceous nenjiang shales from Songliao Basin, northeast China. *Nat. Gas. Geosci.* 35 (1), 119–132. doi:10.11764/j.issn.1672-1926.2023.07.018

Zhang, K., Meng, Z. P., Liu, S. M., Hao, H. J., and Chen, T. (2021a). Laboratory investigation on pore characteristics of coals with consideration of various tectonic deformations. *J. Nat. Gas Sci. Eng.* 91, 103960. doi:10.1016/j.jngse.2021.103960

Zhang, M., Duan, C. C., Li, G. F., Fu, X. H., Zhong, Q., Liu, H. H., et al. (2021b). Determinations of the multifractal characteristics of the pore structures of low-middle- and high-rank coal using high-pressure mercury injection. *J. Petroleum Sci. Eng.* 203, 108656. doi:10.1016/j.petrol.2021.108656

Zhang, N., Wang, S., Li, Z., Guo, S., and Wang, R. (2023a). Application of multifractal theory for determination of fluid movability of coal-measure sedimentary rocks using nuclear magnetic resonance (NMR). *Fractal Fract.* 7 (7), 503. doi:10.3390/fractalfract7070503

Zhang, P. F., Lu, S. F., Li, J. Q., Wang, J. J., Zhang, J. J., and Yin, Y. J. (2023b). Pore structure characterizations of shale oil reservoirs with heat treatment: a case study from dongying sag, Bohai Bay Basin, China. *Acs Omega* 8 (29), 26508–26525. doi:10.1021/acsomega.3c03260

Zhang, S. S., Liu, H., Wu, C. F., and Jin, Z. H. (2022). Influence of particle size on pore structure and multifractal characteristics in coal using low-pressure gas adsorption. *J. Petroleum Sci. Eng.* 212, 110273. doi:10.1016/j.petrol.2022.110273

Zhang, Y. H., Chang, J. Q., Jiang, Z. X., Gao, Z. Y., Zhang, C. J., Wang, G. Z., et al. (2024b). Visualization of dynamic micro-migration of shale oil and investigation of shale oil movability by NMRI combined oil charging/water flooding experiments: a novel approach. *Mar. Petroleum Geol.* 165, 106907. doi:10.1016/j.marpetgeo.2024.106907

Zhao, P. Q., Wang, Z. L., Sun, Z. C., Cai, J. C., and Wang, L. (2017). Investigation on the pore structure and multifractal characteristics of tight oil reservoirs using NMR measurements: Permian Lucaogou Formation in Jimusaer Sag, Junggar Basin. *Mar. Petroleum Geol.* 86, 1067–1081. doi:10.1016/j.marpetgeo.2017.07.011

Zhao, R. X., Xue, H. T., Lu, S. F., Li, J. Q., Tian, S. S., Wang, M., et al. (2022). Multi-scale pore structure characterization of lacustrine shale and its coupling relationship with material composition: an integrated study of multiple experiments. *Mar. Petroleum Geol.* 140 (5), 105648. doi:10.1016/j.marpetgeo.2022.105648

Zheng, S. J., Yao, Y. B., Liu, D. M., Cai, Y. D., Liu, Y., and Li, X. W. (2019). Nuclear magnetic resonance T2 cutoffs of coals: a novel method by multifractal analysis theory. *Fuel* 241, 715–724. doi:10.1016/j.fuel.2018.12.044

Zhou, L., and Kang, Z. H. (2016). Fractal characterization of pores in shales using NMR: a case study from the lower cambrian niutitang Formation in the middle yangtze platform, southwest China. *J. Nat. Gas Sci. Eng.* 35 (9), 860–872. doi:10.1016/j.jngse.2016.09.030

Zhu, B. Y., Meng, J. H., Pan, R. F., Song, C., Zhu, Z. P., Jin, J. E., et al. (2023). Multi-scale characterization of organic matter pore space in deep marine shale combined with mathematical morphology. *Geoenergy Sci. Eng.* 223, 211539. doi:10.1016/j.geoen.2023.211539